A New Statistical Channel Model for Emerging Wireless Communication Systems

ADEBOLA OLUTAYO (Student Member, IEEE), JULIAN CHENG (Senior Member, IEEE), AND JONATHAN F. HOLZMAN (Member, IEEE)

School of Engineering, University of British Columbia, Kelowna, BC V1V 1V7, Canada

CORRESPONDING AUTHOR: A. OLUTAYO (e-mail: adebola.olutayo@alumni.ubc.ca)

ABSTRACT A new composite fading model is introduced. This shadowed Beaulieu-Xie model is developed to characterize wireless communication in an environment with an arbitrary number of line-of-sight and non-line-of-sight signals, in contrast to the existing Rayleigh, Ricean, generalized Ricean (i.e., $\kappa - \mu$), and Nakagami-m models. The proposed model benefits from four parameters that characterize a wide range of fading conditions, unlike existing composite models such as the shadowed Ricean model, the two-wave with diffuse power model, and the fluctuating two-ray model. The proposed shadowed Beaulieu-Xie model is used here to characterize experimental data obtained from fading measurements in 28 GHz outdoor millimeter-wave channels, and it is found to describe the communication environment accurately. We conclude that the proposed composite fading model is particularly useful for characterizing emerging (millimeter-wave and terahertz) wireless communication systems.

INDEX TERMS Beaulieu-Xie distribution, bit-error rate, channel model, emerging systems, fading models, mmwave, non-central chi distribution, outage probability, terahertz.

I. INTRODUCTION

NEW FORMS of wireless systems are emerging to meet the growing demand for mobile communications [1]. Of particular interest are the millimeter wave (mmWave) and terahertz (THz) wireless communication systems, which increase capacity by pushing beyond the traditional microwave spectrum. Such systems hold great promise, but their channels can be challenging to characterize and ultimately understand. This is because they demand a model of fading that offers both flexibility, in terms of adaptable parameters, and compatibility, in accommodating signal transmission via line-of-sight (LOS)[1] and non-line-of-sight (NLOS) components. Contemporary models, such as the Rayleigh, Ricean, generalized Ricean (i.e., κ-μ), and Nakagami-m models, are limited in their ability to provide the required flexibility and LOS/NLOS compatibility.

The Rayleigh fading model has been used to characterize a wide range of communication environments. However, its

fixed (two) degrees of freedom limit its flexibility in describing wireless communication environments. Moreover, it is incapable of characterizing transmission via LOS components, because it is based upon the central chi-distribution. Thus, it cannot support the needed LOS/NLOS compatibility.

The Ricean and generalized Ricean (i.e., κ-μ) distributions [4] are obtained from the non-central chi-distribution and are thus able to characterize transmission via LOS and NLOS components. They have gained notoriety because of this LOS/NLOS compatibility. However, the Ricean fading model only has two degrees of freedom and is therefore limited in its flexibility for characterizing a broad range of signal fades [5]. The generalized Ricean (i.e., κ-μ) model, in contrast, has $2n$ degrees of freedom, where n is the number of independent Gaussian random variables (RVs) and is thus flexible. However, it is not a meaningful fading model because it does not satisfy the power constraint, i.e., its fading power is unbounded [9]. This is evident from its second moment (or the instantaneous power) and parameter, K, in the generalized Ricean model, or κ in the κ-μ model, for which changes to the severity of fading demand adjustments

---

1. Throughout this work, the term LOS will be used to refer to signal transmission via direct propagation and/or specular reflections.

to these parameters to keep the total power of the scatter component invariant.

The Nakagami-m model is a beneficial model in that it can characterize communication environments with multiple NLOS components by way of its flexible fading parameter, m. However, it is derived from the central chi-distribution via normalization and thus cannot characterize LOS components. Notable attempts have been made to apply the Nakagami-m model to environments with both LOS and NLOS components, for the needed LOS/NLOS compatibility, but they have been unsuccessful [8]–[10].

The two-wave with diffuse power fading model [11] can characterize an environment with two dominant LOS components together with NLOS components. However, the probability density function (PDF) and cumulative distributive function (CDF) of its signal envelope are complicated and have no closed-form expressions. Hence, its application for performance analysis of communication systems is limited.

In light of the abovementioned challenges, various composite models have been proposed to characterize the random fluctuations suffered by the received signal given LOS and NLOS components. For example, the shadowed Ricean fading model [12], which considers only a shadowed LOS component, the fluctuating two-ray (FTR) fading model [13], which is limited to two fluctuating LOS components, the κ-μ shadowed distribution [14], whose parent PDF is not meaningful in characterizing fading environments, and the Loo's model [15], whose PDF is not known in closed-form because the LOS signal has a lognormal distribution. Details of more composite models can be found in [12]. Ultimately, all of these composite models have one or more limitations in characterizing fading environments with both LOS and NLOS components.

Given the above search for a fading model that offers both flexibility and LOS/NLOS compatibility, a new model was recently proposed by Beaulieu and Xie [6]. The BX fading model, as it will be referred to in this work, unifies the Rayleigh, Ricean, generalized Ricean (i.e., κ-μ), and Nakagami-m distributions. It is derived from the non-central chi-distribution, in the same manner by which the Nakagami-m distribution was derived from the central chi-distribution, via normalization. The normalization is carried out by scaling a RV that is described by the non-central chi distribution to create a new distribution in the form of the BX fading model. Ultimately, this normalization ensures that the BX fading model does not violate the physical principle of the scatter component invariance, unlike the generalized Ricean (i.e., κ-μ) distribution. Moreover, the BX fading model exhibits flexibility by way of its parameter m.

The seamless relationships that exist between the Rayleigh, Ricean, Nakagami-m, and BX models are presented in Figure 1. The Nakagami-m model is a particular case of the BX fading model in the absence of the LOS component, just as the Ricean fading model becomes the Rayleigh fading model in the absence of the LOS component. Also, the BX fading model becomes the Ricean fading
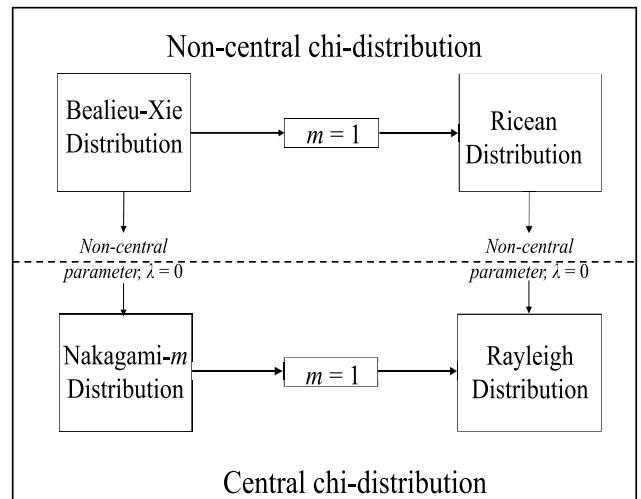

FIGURE 1. Relationships between the Rayleigh, Ricean, Nakagami-m, and BX models. The parameters m and λ represent the fading severity parameter and non-centrality parameter, respectively.

model when m equals to one just as the Nakagami-m model becomes the Rayleigh fading model when m equals to one.

In this work, we introduce a new composite model, based on the BX fading model, which we refer to as the shadowed BX fading model. We assume that the amplitude of the LOS components is Nakagami-m distributed,[2] which makes its power a Gamma RV. While other composite models that assumed the LOS components to be fluctuating according to the Nakagami-m model did not justify their choice [12], [13], we will justify our assumption of Nakagmi-m distributed LOS component as follows. Our assumption of a varying LOS signal envelope is based upon physical insight. The physical fading environment causes the received signal power to fluctuate in time and space as a result of shadowing and multipath fading [7]. Multipath fading arises as a result of signal components traveling to the receiver via different paths. When the received signal is a combination of multiple LOS plus NLOS components, we have the envelope become BX distributed [6]. However, a partial or complete blockage of the LOS components can induce random variations to the amplitude of the received signal. It should be noted that shadowing is only considered for the LOS components here because these components are concentrated in beams over narrow solid angles, i.e., small cross-sectional areas, making them preferentially sensitive to degradation from impinging obstructions. This is in contrast to the NLOS components, which are far less susceptible to degradation from impinging obstructions simply because they are distributed over wide solid angles, i.e., large cross-sectional areas. Ultimately, the received signal envelope from this combination of random variations of the LOS and NLOS power presents an envelope not describable by

2. The Nakagami-m random variable (RV) is assumed for describing the fluctuating LOS components because its probability density function (PDF) offers analytical tractability. We have investigated the shadowed BX model using the BX PDF, but we found it to be analytically intractable.

the abovementioned unimodal and bimodal distributions. The new shadowed BX model overcomes this challenge by incorporating distinct parameters to describe the fading and shadowing severities in the LOS and NLOS signals. This comes about because the constituent Nakagami-*m* and BX models exhibit flexibility by way of their parameters, m_Y and m, respectively. Moreover, the shadowed BX model remains valid when there are more than two LOS components. This is a key feature that other composite models do not incorporate. In this work, we obtain the chief probability functions of this new model in terms of relatively simple (hypergeometric) functions. To justify our claim that the shadowed BX model can be more effective than other fading models, especially in emerging systems, we fit its distribution to field measurements from [3].

The remainder of the paper is organized as follows. In Section I, we introduce the system model of the shadowed BX model. The physical model of the shadowed BX model is presented in Section II. We derive its first-order statistics in Section III, including the PDF of the envelope and instantaneous power, the CDF and the characteristic function (CHF) of the envelope, the moments of the PDF, and the moment generating function (MGF) of the instantaneous power.

In Section IV, we present the fit of the shadowed BX model to measurements. We derive closed-form expressions of the error rates and outage probability (OP) in Section V while considering noncoherent and coherent detections. Section VI presents and discusses the numerical results. Concluding remarks are given in Section VII.

II. PHYSICAL MODEL
The shadowed BX model introduced in this work is based upon the BX fading model. The BX fading model was introduced in a bid to characterize an environment with multiple LOS (direct and specular) components and NLOS (diffuse) components in a more meaningful manner than the generalized Ricean (i.e., κ-μ) distribution [6], while keeping some characteristics of the generalized Ricean (i.e., κ-μ) distribution.

For these models, the noncentral chi RV follows

$$Z = \sqrt{\sum_{i=1}^{k}\left(\frac{X_i}{\sigma_i}\right)^2} \qquad (1)$$

where X_i is a Gaussian RV with a non-zero mean μ_i and variance σ_i^2. The PDF of the RV Z takes the form of

$$f_Z(z) = \frac{\exp\left(-\frac{z^2+\lambda^2}{2}\right)z^k\lambda}{(\lambda z)^{\frac{k}{2}}} I_{\frac{k}{2}-1}(\lambda z) \qquad (2)$$

where k is the degree of freedom, λ is the noncentral parameter, which is related to the mean of X_i by $\lambda = \sqrt{\sum_{i=1}^{k}\mu_i^2}$, and $I_v(\cdot)$ is the vth-order modified Bessel function of the first kind. The BX fading model is obtained from the noncentral chi distribution in (2) via normalization by a factor

$\sqrt{\frac{2m}{\Omega}}$ while noting the relation of $k = 2m$, to have a new RV D distributed according to the BX fading model

$$f_D(d) = \frac{\exp\left(-\frac{m}{\Omega}(d^2+\lambda^2)\right)d^m\left(\frac{2m}{\Omega}\right)}{\lambda^{m-1}} I_{m-1}\left(\frac{2m}{\Omega}\lambda d\right) \qquad (3)$$

where m is the BX shape parameter, λ^2 is the power of LOS component, and Ω is the power of the NLOS components. It is important to note that the noncentral parameter λ in (2) is also scaled by the factor $\sqrt{\frac{2m}{\Omega}}$ such that the λ in (3), which for clarity we refer to as λ^*, becomes $\lambda = \lambda^*\sqrt{\frac{2m}{\Omega}}$.

For the shadowed BX model introduced in this paper, we assume that λ in (3) is fluctuating because of the dynamic nature of the channel. Hence, we use another RV, Y, to represent the fluctuating LOS amplitude, λ. The PDF of the new composite model can then be expressed as

$$f_R(r) = E_Y\left[\frac{2m_X}{\Omega_X}\frac{r^{m_X}}{y^{m_X-1}}\exp\left(-\frac{m_X}{\Omega_X}\left(r^2+y^2\right)\right)\right.$$
$$\left.\times I_{m_X-1}\left(\frac{2m_X}{\Omega_X}yr\right)\right] \qquad (4)$$

where $E_Y[\cdot]$ denotes the expectation with respect to Y and Ω_X is the average power of the NLOS component due to multipath effects. The fading parameter, m_X, characterizes the level to which both the LOS and NLOS signals are subject to fading. This parameter can take on values in the range of $m_X > 0$ in the shadowed BX model, characterizing severe fading at low m_X values to little fading at high m_X values. This is in contrast to the traditional BX fading model, where the fading parameters can only take on values from 0.5. Note that the argument of the expectation operator in (4) is the PDF of the BX fading model.

III. STATISTICAL CHARACTERIZATION
In this section, we obtain expressions for the chief probability functions of the proposed shadowed BX model in closed-form. The goal here is to create an accurate statistical model of the communication environment—with realistic and physical parameters characterizing the environmental effects. It then becomes possible to understand and overcome impairments in the system during the design, simulation, and testing. For this statistical model, the LOS and NLOS components are assumed to experience different forms and levels of fluctuations, as is often seen in practice. The fluctuations are quantified by separate shadowing and fading severity parameters for both the LOS and NLOS signals.

The PDF of the envelope of the shadowed BX model is

$$f_R(r) = \int_0^\infty \frac{2m_X}{\Omega_X}\frac{r^{m_X}}{y^{m_X-1}}\exp\left(-\frac{m_X}{\Omega_X}\left(r^2+y^2\right)\right)$$
$$\times I_{m_X-1}\left(\frac{2m_X}{\Omega_X}yr\right)f_Y(y)dy \qquad (5)$$

with $f_Y(y)$ being the Nakagami-*m* PDF

$$f_Y(y) = \frac{2m_Y^{m_Y}}{\Gamma(m_Y)\Omega_Y^{m_Y}}y^{2m_Y-1}\exp\left(-\frac{m_Y y^2}{\Omega_Y}\right), \quad y \geq 0 \qquad (6)$$

where $\Gamma(\cdot)$ is the gamma function, Ω_Y is the average power of the LOS components, and m_Y is the shadowing parameter. This latter parameter characterizes the level to which the LOS components are subject to shadowing, and it defines the number of the LOS components as $2m_Y$. It can take on values in the range of $m_Y \geq 0$, characterizing LOS shadowing from a limiting case of complete obstruction that could be seen in a dense urban environment to partial/no obstruction that could be seen in a suburban/open environment. Thus, the range of m_Y for the shadowed BX model is broader than that of the traditional Nakagami-m model, making it better suited for characterizing severe shadowing. It should be noted that shadowing depends upon the positions of the transmitter and receiver, as well as the positions (and materials) of obstacles in the environment. This means that shadowing, and its impact on the LOS components, would have no preferential direction in a generalized wireless communication environment. Therefore, one can, at best, use a statistical characterization for the net result of shadowing on all LOS components. This is done with the single parameter m_Y in the proposed model. At the same time, the physicality of the proposed model can be seen by the fact that it satisfies the physical constraint of power conversation, i.e., it has a bounded fading power. This will be shown by its second-order moment, which is independent of the parameters m_X and m_Y. Thus, its constituent BX PDF becomes an impulse at a constant value of $\sqrt{\lambda^2 + \Omega}$, as the parameter m approaches infinity, and its constituent Nakagami-m PDF becomes an impulse at a constant value of $\sqrt{\Omega_Y}$, as the parameter m_Y approaches infinity. It is also worth noting that the Nakagami-m distribution characterizes the fluctuating LOS components with a fading power that is bounded, and it does so with a PDF that allows for straightforward mathematical manipulations/expressions via chief probability functions.

By solving (5) according to [16, p. 706], the PDF of the envelope of the shadowed BX model is obtained as (7), as shown at the bottom of the page, where $K = \frac{\Omega_Y}{\Omega_X}$ is the K-factor given Ω_Y as the LOS power and Ω_X as the NLOS power, and $_1F_1(\cdot; \cdot; \cdot)$ is the confluent hypergeometric function defined as [16, p. 1023]

$$_1F_1(a; b; w) = \sum_{n=0}^{\infty} \frac{(a)_n}{(b)_n} \frac{w^n}{n!}, \quad (a)_n = \frac{\Gamma(a+n)}{\Gamma(a)}. \quad (8)$$

We observe that the PDF of the shadowed BX model in (7) is expressed in terms of $_1F_1(\cdot; \cdot; \cdot)$, which can be obtained with standard mathematical software.

Inserting (8) into (7), the CDF of the shadowed BX model, defined by $F_R(r) = \int_0^r f_R(t)dt$, is obtained as

$$F_R(r) = \frac{2}{\Gamma(m_Y)} \left(\frac{m_X}{\Omega_X}\right)^{m_X} \left(\frac{m_Y \Omega_X}{m_X \Omega_Y + m_Y \Omega_X}\right)^{m_Y}$$
$$\times \sum_{n=0}^{\infty} \frac{\Gamma(m_Y + n)}{n! \Gamma(m_X + n)} \left(\frac{m_X^2 \Omega_Y}{\Omega_X(m_X \Omega_Y + m_Y \Omega_X)}\right)^n$$
$$\times \int_0^r t^{2(m_X+n)-1} \exp\left(-\frac{m_X}{\Omega_X}t^2\right)dt. \quad (9)$$

After some algebraic manipulations, the CDF is ultimately obtained as

$$F_R(r) = \frac{1}{\Gamma(m_Y)} \left(\frac{m_X}{\Omega_X}\right)^{m_X} \left(\frac{m_Y \Omega_X}{m_X \Omega_Y + m_Y \Omega_X}\right)^{m_Y}$$
$$\times \sum_{n=0}^{\infty} \frac{\Gamma(m_Y + n)}{n! \Gamma(m_X + n)} \left(\frac{m_X \Omega_Y}{m_X \Omega_Y + m_Y \Omega_X}\right)^n$$
$$\times g\left(m_X + n, \frac{m_X}{\Omega_X}r^2\right) \quad (10)$$

where $g(v, u)$ is the incomplete gamma function given by [19]

$$g(v, u) = \int_0^u b^{v-1} \exp(-b)db, \quad v > 0$$
$$= v^{-1}u^v {}_1F_1(v; 1+v; -u). \quad (11)$$

The moments of the PDF in (7) are

$$E\left[R^k\right] = \int_{-\infty}^{\infty} r^k f_R(r)dr$$
$$= \left(\frac{m_Y \Omega_X}{m_X \Omega_Y + m_Y \Omega_X}\right)^{m_Y} \frac{\Gamma\left(m_X + \frac{k}{2}\right)}{\Gamma(m_X)} \left(\frac{m_X}{\Omega_X}\right)^{-\frac{k}{2}}$$
$$\times {}_2F_1\left(m_X + \frac{k}{2}, m_Y; m_X; \frac{m_X \Omega_Y}{m_X \Omega_Y + m_Y \Omega_X}\right) \quad (12)$$

where the Gauss hypergeometric function is defined as [21]

$$_2F_1(a, b; c; z) = \sum_{n=0}^{\infty} \frac{(a)_n (b)_n}{(c)_n} \frac{z^n}{n!}, \quad (a)_n = \frac{\Gamma(a+n)}{\Gamma(a)}, \quad (13)$$

which converges if c is a positive value for all of $|z| < 1$. Note that the Gauss hypergeometric function is also available in standard mathematical software. The characteristic function (CHF) of any distribution is defined to be [22]

$$\Phi_R(\omega) = \int_{-\infty}^{\infty} f_R(r)e^{j\omega r}dr. \quad (14)$$

$$f_R(r) = \frac{2}{\Gamma(m_X)} \left(\frac{m_Y \Omega_X}{m_X \Omega_Y + m_Y \Omega_X}\right)^{m_Y} \left(\frac{m_X}{\Omega_X}\right)^{m_X} r^{2m_X-1} {}_1F_1\left(m_Y; m_X; \frac{m_X^2 \Omega_Y r^2}{\Omega_X(m_X \Omega_Y + m_Y \Omega_X)}\right) \exp\left(-\frac{m_X r^2}{\Omega_X}\right) \quad (7)$$

For our model, we apply the Taylor series expansion to $e^{j\omega r}$, so that the CHF of the shadowed BX model can be obtained in terms of an infinite series as

$$
\begin{aligned}
\Phi_R(\omega) &= \sum_{k=0}^{\infty} \frac{(j\omega)^k}{k!} E\{R^k\} \\
&= \sum_{k=0}^{\infty} \frac{(j\omega)^k}{k!} \left(\frac{m_Y \Omega_X}{m_X \Omega_Y + m_Y \Omega_X} \right)^{m_Y} \frac{\Gamma\left(m_X + \frac{k}{2}\right)}{\Gamma(m_X)} \\
&\quad \times {}_2F_1\left(m_X + \frac{k}{2}, m_Y; m_X; \frac{m_X \Omega_Y}{m_X \Omega_Y + m_Y \Omega_X} \right) \\
&\quad \times \left(\frac{m_X}{\Omega_X} \right)^{-\frac{k}{2}}.
\end{aligned}
\tag{15}
$$

Equation (15) is a convergent infinite series representation of the CHF, which can also be computed using the NIntegrate function in Mathematica software directly from (14).

We go on to define the instantaneous power as $S(t) = R^2(t)$ [12], whose PDF is obtained by making the substitution $f_S(\gamma) = \frac{1}{2r} f_r(r)$ to have

$$
\begin{aligned}
f_S(\gamma) &= \frac{1}{\Gamma(m_X)} \left(\frac{m_Y \Omega_X}{m_X \Omega_Y + m_Y \Omega_X} \right)^{m_Y} \left(\frac{m_X}{\Omega_X} \right)^{m_X} \gamma^{m_X - 1} \\
&\quad \times {}_1F_1\left(m_Y; m_X; \frac{m_X^2 \Omega_Y \gamma}{\Omega_X(m_X \Omega_Y + m_Y \Omega_X)} \right) \\
&\quad \times \exp\left(-\frac{m_X}{\Omega_X} \gamma \right).
\end{aligned}
\tag{16}
$$

The CDF of the instantaneous power plays a vital role in obtaining the OP. We obtain the CDF of the instantaneous power, defined by $F_S(\gamma) = \int_0^{\gamma} f_S(t) dt$, as

$$
\begin{aligned}
F_S(\gamma) &= \left(\frac{m_Y \Omega_X}{m_X \Omega_Y + m_Y \Omega_X} \right)^{m_Y} \sum_{n=0}^{\infty} \frac{\Gamma(m_Y + n)}{n! \Gamma(m_X + n) \Gamma(m_Y)} \\
&\quad \times \left(\frac{m_X \Omega_Y}{m_X \Omega_Y + m_Y \Omega_X} \right)^n g\left(m_X + n, \frac{m_X}{\Omega_X} \gamma \right).
\end{aligned}
\tag{17}
$$

The MGF of the instantaneous power, defined as $M_\gamma(s) = E[\exp(-\gamma s)]$, is obtained as

$$
\begin{aligned}
M_S(\gamma) &= \left(\frac{m_Y \Omega_X}{m_X \Omega_Y + m_Y \Omega_X} \right)^{m_Y} \left(\frac{m_X}{\Omega_X} \right)^{m_X} \\
&\quad \times \sum_{n=0}^{\infty} \frac{\Gamma(m_Y + n)}{n! \Gamma(m_Y)} \left(\frac{m_X^2 \Omega_Y}{\Omega_X(m_X \Omega_Y + m_Y \Omega_X)} \right)^n \\
&\quad \times \left(\gamma + \frac{m_X}{\Omega_X} \right)^{-(m_X + n)}.
\end{aligned}
\tag{18}
$$

The expressions for the chief probability functions shown above are relatively simple, allowing for easy mathematical manipulation and verification via simulations with Mathematica and MATLAB. The CDF and MGF of the instantaneous power shown in (17) and (18) also allow for straightforward calculation of the OP and average bit-error rate (BER), respectively.

TABLE 1. Parameters of the shadowed BX model as they appear in other fading models.
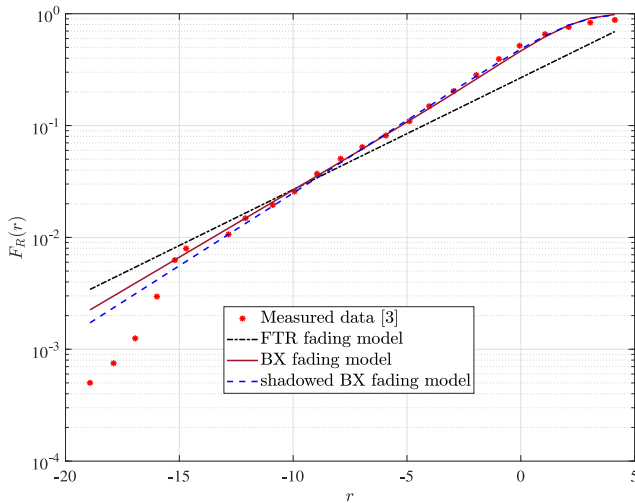
Fading Model	Shadowed BX Parameters
Rayleigh	$m_X = 1, m_Y = 0$
Ricean	$m_X = 1, m_Y = \infty$
One-sided Gaussian	$m_X = 0.5, m_Y = 0$
Beaulieu-Xie [6]	$m_Y = \infty$
Nakagami-m	$m_Y = 0$
Shadowed Ricean [12]	$m_X = 1$

The derived expression for the PDF of the shadowed BX model or the MGF of its SNR can present insight into its diversity order. The diversity order of a statistical model can be obtained by observing the behaviour of its PDF at the origin or the asymptotic behaviour of the MGF of the SNR as the SNR approaches infinity [17]. Equally, for the MGF of the SNR, the slope of the log-log plot of the BER or OP can define the diversity order of a system. The diversity order, manifesting as the slope of a log-log plot for the average bit error rate (BER) versus average signal-to-noise ratio (SNR) or outage probability (OP) versus average SNR, is equal to the fading parameter m_X, which is also associated with the degree of freedom of the shadowed BX model. Appendix A shows the derivation for the diversity order of the shadowed BX from the expression of its BER.

As a final point on statistical characterization, we can identify the relationships between the parameters of the shadowed BX model and other fading models. The relationships are summarized in Table 1. Of particular note is the relationship between the parameter sets of the shadowed BX and Ricean model. The physicality of the shadowed BX model can also be seen by establishing its relevant relationship with the parameter set of the Ricean model. The parameter set of the shadowed BX model, $(m_X, \Omega_X, m_Y, \Omega_Y)$, where m_X is the fading parameter, Ω_X is the power of the NLOS components, m_Y is the shadowing parameter, and Ω_Y is the power of the LOS components, can be linked to the parameter set of the Ricean fading model, $(1, b_0, \infty, \Omega)$, where b_0 sets the power of the NLOS components, and Ω is the power of the LOS components, because the Ricean model is a special case of the shadowed BX model. In fitting the measured data of [3], it is found that the independence of the shadowed BX model's parameters, m_X and m_Y, can better match the concavity and convexity of the given PDF and can provide a better overall fit, in comparison to the Ricean fading model.

IV. FIT TO PUBLISHED MEASUREMENTS

To validate the proposed shadowed BX model for use in emerging wireless systems, we compare its fit to published data, for a mmWave communication environment with small-scale fading in the 28 GHz band [3], against those of the FTR and BX fading models. Fitting can also be done with the Ricean fading model, as employed in [3], but its parameters can instead be extracted from the parameters of the shadowed BX model. The fittings carried out in this section bring a fair comparison between the BX and shadowed BX models and other existing models that have characterized (the same) experimental data, specifically the Ricean [3]

FIGURE 2. Fits of the FTR, BX, and shadowed BX models to empirically obtained signal amplitude [3] for vertical-vertical co-polarized LOS measurements. The FTR fading model has parameters of $m = 80$, $\Delta = 0.6$, and $K_{FTR} = 22$ dB, yielding $KS_{LOS}^{FTR} = 0.1560$. The BX fading model has parameters of $m = 0.6$, $\Omega = 1$ dB, and $\lambda = 0$ dB, yielding $KS_{LOS}^{BX} = 0.0612$. The shadowed BX model has parameters of $m_X = 0.6$, $\Omega_X = 1$ dB, and $\Omega_Y = 0$ dB, yielding $KS_{LOS}^{SBX} = 0.0708$.

FIGURE 3. Fits of the FTR, BX, and shadowed BX models to empirically obtained signal amplitude [3] for vertical-horizontal co-polarized NLOS measurements. The FTR fading model has parameters of $m = 5$, $\Delta = 0.75$, and $K_{FTR} = 12$, yielding $KS_{LOS}^{FTR} = 1.5723$. The BX fading model has parameters of $m = 0.65$, $\Omega = -2$ dB, and $\lambda = 0$ dB, yielding $KS_{NLOS}^{BX} = 0.0595$. The shadowed BX model has parameters of $m_X = 0.65$, $m_Y = 1.95$, $\Omega_X = -2$ dB, and $\Omega_Y = 0$ dB, yielding $KS_{NLOS}^{SBX} = 0.0412$.
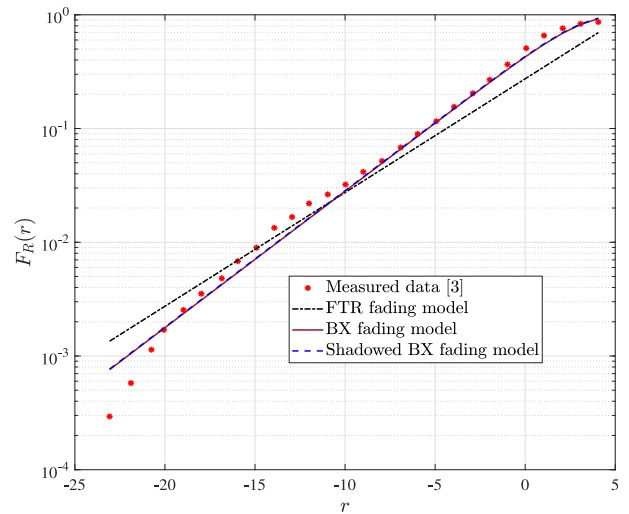
and fluctuating two-ray [13] models. At the same time, such characterizations give insight on the differing functionality of the shadowed BX model and its parent BX model. In doing this, we have found that the combined effects of the parameters m_X and m_Y can better encompass (the more challenging) characteristics with high curvatures and/or inflections leading to better overall fitting.

To carry out the fitting, we compare the analytical CDF of the envelope of our composite model, $F_R(r)$, with the empirical CDF of the published data, $\hat{F}_R(r)$. We obtain the most suitable parameter values for minimized error between these CDFs and quantify the deviation of the analytical CDFs from the empirical CDF using the Kolmogorov-Smirnov (KS) test [11] in two ways. Parameter values from existing measurements, characterized according to the Ricean fading model in [3], were obtained by establishing and applying the relevant expressions linking the parameters of the shadowed BX model and those of the Ricean fading model. Parameter values that were not based upon existing measurements were obtained by a grid search that minimizes the KS test value. The KS test is given as

$$KS \triangleq \max \left| \hat{F}_R(r) - F_R(r) \right| \tag{19}$$

where $|\cdot|$ is the absolute value operator. Based upon the definition in (19), the smaller the value of KS, the better the fit of the analytical CDF to the empirical CDF obtained from the measured data.

Figure 2 compares the empirical CDF obtained from the vertical-vertical co-polarized LOS measurements in [3] with the analytical CDFs of the FTR, the BX, and the shadowed BX models. The analytical CDFs for these fading models are seen to fit the measured data closely. However, the BX fading model provides a better fit. This is because the measured data was obtained in a setting where there was no obstruction

to the signals traveling from the transmitter to the receiver, i.e., there was no shadowing or fluctuations to the LOS component. The absence of shadowing was confirmed in the PDF of the shadowed BX model, which remains unchanged despite making significant changes to the value of m_Y (quantifying the shadowing severity). The goodness-of-fit for the three models are calculated using (19), which gives $KS_{LOS}^{FTR} = 0.1560$, $KS_{LOS}^{BX} = 0.0612$, and $KS_{LOS}^{SBX} = 0.0708$, respectively. Ultimately, the BX fading model shows its advantage in fitting an environment that is free of shadowing. In addition, the results in Fig. 2 confirm that the shadowed BX model indeed reduces to the BX fading model when $m_Y \to \infty$.

Figure 3 provides a comparison between the empirical CDF for vertical-horizontal co-polarized NLOS measurements in [3] with the analytical CDFs of the FTR, BX, and shadowed BX models. The goodness-of-fit is obtained using (19) as $KS_{NLOS}^{FTR} = 1.5723$ for the FTR model, $KS_{NLOS}^{BX} = 0.0595$ for the BX model, and $KS_{NLOS}^{SBX} = 0.0412$ for the shadowed BX model. Here, the shadowed BX model provides a better fit. This is because the LOS components experience fluctuations as a result of varying channel characteristics, and the shadowed BX fading model best characterizes these LOS fluctuations.

It should be noted that the value of each data point in the measured CDF is based upon (i) the individual multipath component in the bin over the local area and (ii) the amplitude of the previous data point considering that the distribution is cumulative. Thus, the performance of the shadowed BX model when characterizing the measured data in the low r regime is based on the above-mentioned point. Also, in Fig. 2, the amplitude fluctuations over the local area that produces the values below -15 dB are very high, indicating significant fading, in comparison to the

lower amplitude fluctuations that lead to higher values above -15 dB. In Fig. 3, the CDF of the measured data deviates far less from the analytical CDF because the measured data was obtained for an environment with prevalent NLOS propagation. Thus, the local areas are rich in multipath signal components, leading to higher amplitude values and better overall fits in the figure.

V. PERFORMANCE ANALYSIS

In this section, we present performance results for the average BER and OP. Owing to the fact that the shadowed BX model has simple expressions for its first-order statistics and those related to the signal-to-noise ratio (SNR), the results for the BER and OP are obtained with minimal mathematical manipulations.

A. AVERAGE BIT-ERROR RATE

In this section, we calculate the average BER, $\bar{P}_E$, which is defined as the conditional error probability, $P_e(\gamma)$, averaged over the output SNR in an additive white Gaussian noise (AWGN) channel. It is given as

$$\bar{P}_E = \int_0^\infty P_e(\gamma) f_S(\gamma) \, d\gamma \tag{20}$$

where $f_S(\gamma)$ is the PDF of the SNR as obtained in (16). We continue in the following subsections by deriving the expressions for noncoherent and coherent detections.

1) NONCOHERENT DETECTION

The average BER in (20) is defined for noncoherent frequency-shift keying (FSK) or differential phase-shift keying (PSK) detections as [19]

$$P_e(\gamma) = \frac{1}{2} \exp(-\varpi \gamma), \tag{21}$$

where

$$\varpi = \begin{cases} 1, & \text{for binary PSK} \\ \frac{1}{2}, & \text{for binary FSK}. \end{cases} \tag{22}$$

Substituting (16) and (21) into (20), we have

$$\bar{P}_E = \frac{1}{2\Gamma(m_X)} \left(\frac{m_Y \Omega_X}{m_X \Omega_Y + m_Y \Omega_X} \right)^{m_Y} \left(\frac{m_X}{\Omega_X} \right)^{m_X}$$
$$\times \int_0^\infty \gamma^{m_X - 1} {}_1F_1\left(m_Y; m_X; \frac{m_X^2 \Omega_Y \gamma}{\Omega_X(m_X \Omega_Y + m_Y \Omega_X)} \right)$$
$$\times \exp\left[-\left(\frac{m_X}{\Omega_X} + \varpi \right) \gamma \right] \tag{23}$$

where ${}_1F_1(\cdot; \cdot; \cdot)$ is defined in (8). Using [16, p. 822], the average BER for noncoherent detection is obtained as

$$\bar{P}_E = \frac{1}{2} \left(\frac{m_Y \Omega_X}{m_X \Omega_Y + m_Y \Omega_X} \right)^{m_Y} \left(\frac{m_X}{m_X + \varpi \Omega_X} \right)^{m_X}$$
$$\times {}_2F_1\left(m_Y, m_X; m_X; \frac{m_X^2 \Omega_Y}{(m_X + \varpi \Omega_X)(m_X \Omega_Y + m_Y \Omega_X)} \right) \tag{24}$$

where ${}_2F_1(\cdot, \cdot; \cdot; \cdot)$ is defined in (13).

2) COHERENT DETECTION

For coherent detections, $P_e(\gamma)$ is defined as [19]

$$P_e(\gamma) = \frac{1}{2} \operatorname{erfc}\left(\sqrt{\varpi \gamma} \right) \tag{25}$$

where ϖ is defined in (22) and erf*c* is the complementary error function defined in terms of the upper incomplete gamma function as

$$\operatorname{erfc}(x) = \frac{\Gamma\left(\frac{1}{2}, x^2 \right)}{2\sqrt{\pi}}. \tag{26}$$

Inserting (16) and (26) into (20) gives

$$\bar{P}_E = \frac{1}{2\sqrt{\pi}\Gamma(m_X)} \left(\frac{m_Y \Omega_X}{m_X \Omega_Y + m_Y \Omega_X} \right)^{m_Y} \left(\frac{m_X}{\Omega_X} \right)^{m_X}$$
$$\times \sum_{n=0}^\infty \frac{\Gamma(m_Y + n)}{n! \Gamma(m_Y)} \frac{\Gamma(m_X)}{\Gamma(m_X + n)} \left(\frac{m_X^2 \Omega_Y}{\Omega_X(m_X \Omega_Y + m_Y \Omega_X)} \right)^n$$
$$\times \int_0^\infty \gamma^{m_X + n - 1} \exp\left(-\frac{m_X}{\Omega_X} \gamma \right) \Gamma\left(\frac{1}{2}, \varpi \gamma \right) d\gamma. \tag{27}$$

Using [16, p. 657], we obtain the average BER for coherent detection as

$$\bar{P}_E = \frac{\sqrt{\varpi}}{2\sqrt{\pi}} \left(\frac{m_Y \Omega_X}{m_X \Omega_Y + m_Y \Omega_X} \right)^{m_Y} \left(\frac{m_X}{\Omega_X} \right)^{m_X}$$
$$\times \sum_{n=0}^\infty \frac{\Gamma(m_Y + n)}{n! \Gamma(m_Y)} \times \left(\frac{m_X^2 \Omega_Y}{m_X \Omega_Y + m_Y \Omega_X} \right)^n$$
$$\times \frac{\Gamma\left(m_X + n + \frac{1}{2} \right)}{\Gamma(m_X + n + 1)} \times \left(\frac{\Omega_X}{\varpi \Omega_X + m_X} \right)^{m_X + n + \frac{1}{2}}$$
$$\times {}_2F_1\left(1, m_X + n + \frac{1}{2}; m_X + n + 1; \frac{m_X}{\varpi \Omega_X + m_X} \right) \tag{28}$$

where ${}_2F_1(\cdot, \cdot; \cdot; \cdot)$ is defined in (13). We observe from our results of the average BER with coherent detection that the relative error drops from 1 percent to 0.5 percent when the number of terms that are applied in the summations is increased from 50 to 100. We show in Appendix B that the result in (28) approaches zero as n approaches infinity. The error in truncating the infinite series in (28) is given by

$$\epsilon_C = \frac{\sqrt{\varpi}}{2\sqrt{\pi}} \left(\frac{m_Y \Omega_X}{m_X \Omega_Y + m_Y \Omega_X} \right)^{m_Y} \left(\frac{m_X}{\Omega_X} \right)^{m_X}$$
$$\times \sum_{n=N}^\infty \frac{\Gamma(m_Y + n)}{n! \Gamma(m_Y)} \left(\frac{m_X^2 \Omega_Y}{m_X \Omega_Y + m_Y \Omega_X} \right)^n$$
$$\times \frac{\Gamma\left(m_X + n + \frac{1}{2} \right)}{\Gamma(m_X + n + 1)} \times \left(\frac{\Omega_X}{\varpi \Omega_X + m_X} \right)^{m_X + n + \frac{1}{2}}$$
$$\times {}_2F_1\left(1, m_X + n + \frac{1}{2}; m_X + n + 1; \frac{m_X}{\varpi \Omega_X + m_X} \right). \tag{29}$$

After some algebraic manipulation, the truncation error expressed in (29) can be bounded by

$$
\epsilon_C \leq \frac{\sqrt{\varpi}}{2\sqrt{\pi}\,\Gamma(m_Y)} \left(\frac{m_Y\Omega_X}{m_X\Omega_Y + m_Y\Omega_X}\right)^{m_Y} \left(\frac{m_X}{\Omega_X}\right)^{m_X}
$$

$$
\times \left(\varpi + \frac{m_X}{\Omega_X}\right)^{-\left(m_X + N + \frac{1}{2}\right)} \left(\frac{m_X^2\Omega_Y}{m_X\Omega_Y + m_Y\Omega_X}\right)^{N}
$$

$$
\times_2 F_1\left(1, m_X + N + \frac{1}{2}; m_X + N + 1; \frac{m_X}{\varpi\,\Omega_X + m_X}\right)
$$

$$
\times \frac{\Gamma(m_Y + N - 1)\Gamma\left(m_X + N + \frac{1}{2}\right)}{\Gamma(m_X + N)}
$$

$$
\times_2 F_2\left(m_Y + N, m_X + N + \frac{1}{2}; N + 1, m_X + N + 1;\right.
$$

$$
\left. \times \frac{m_X^2\Omega_Y}{m_X\Omega_Y + m_Y\Omega_X}\right) \quad (30)
$$

where $_2F_2(\cdot, \cdot; \cdot, \cdot; \cdot)$ is the generalized hypergeometric function, $_pF_q(a_1, \ldots, a_p; b_1, \ldots, b_q; z)$, with $p = 2$ and $q = 2$ [16].

B. OUTAGE PROBABILITY

The mathematical derivation for the OP is provided in this section. The OP is defined as the probability that the SNR falls below a given threshold level, γ_b [7], or the probability by which the BER is greater than a specified threshold level, P_e^* [19]. It is given by

$$
P_{out} = p(\gamma < \gamma_b) = \int_0^{\gamma_b} f_S(\gamma)\ d\gamma, \quad (31)
$$

where

$$
\gamma_b = \begin{cases} -\frac{1}{\varpi}\ln\left(2P_e^*\right), & \text{for noncoherent detection} \\ \frac{1}{\varpi}\mathrm{erfc}^{-1}\left(2P_e^*\right), & \text{coherent detection.} \end{cases} \quad (32)
$$

Inserting (16) into (31), we have

$$
P_{out} = \frac{1}{\Gamma(m_X)} \left(\frac{m_Y\Omega_X}{m_X\Omega_Y + m_Y\Omega_X}\right)^{m_Y} \left(\frac{m_X}{\Omega_X}\right)^{m_X}
$$

$$
\times \int_0^{\gamma_b} \gamma^{m_X - 1} \exp\left(-\frac{m_X}{\Omega_X}\gamma\right)
$$

$$
\times_1 F_1\left(m_Y; m_X; \frac{m_X^2\Omega_Y\gamma}{\Omega_X(m_X\Omega_Y + m_Y\Omega_X)}\right) d\gamma. \quad (33)
$$

According to the definition of the confluent hypergeometric function expressed in (8) to (33), the OP becomes

$$
P_{out} = \frac{1}{\Gamma(m_X)} \left(\frac{m_Y\Omega_X}{m_X\Omega_Y + m_Y\Omega_X}\right)^{m_Y} \left(\frac{m_X}{\Omega_X}\right)^{m_X}
$$

$$
\times \sum_{n=0}^{\infty} \frac{\Gamma(m_Y + n)\Gamma(m_X)}{n!\,\Gamma(m_X + n)\Gamma(m_Y)} \left(\frac{m_X^2\Omega_Y}{\Omega_X(m_X\Omega_Y + m_Y\Omega_X)}\right)^{n}
$$

$$
\int_0^{\gamma_b} \gamma^{m_X + n - 1} \exp\left(-\frac{m_X}{\Omega_X}\gamma\right) d\gamma. \quad (34)
$$

Using [16, p. 346], we obtain the OP as

$$
P_{out} = \left(\frac{m_Y\Omega_X}{m_X\Omega_Y + m_Y\Omega_X}\right)^{m_Y} \sum_{n=0}^{\infty} \frac{\Gamma(m_Y + n)}{n!\,\Gamma(m_X + n)\Gamma(m_Y)}
$$

$$
\times \left(\frac{m_X\Omega_Y}{m_X\Omega_Y + m_Y\Omega_X}\right)^{n} g\left(m_X + n, \frac{m_X}{\Omega_X}\gamma_b\right), \quad (35)
$$

where $g(\cdot, \cdot)$ is the lower incomplete gamma function defined in (11). We show in Appendix C that the result in (35) approaches zero as n approaches infinity. The error in truncating the infinite series in (35) is given by

$$
\epsilon_{OP} = \left(\frac{m_Y\Omega_X}{m_X\Omega_Y + m_Y\Omega_X}\right)^{m_Y} \sum_{n=N}^{\infty} \frac{\Gamma(m_Y + n)}{n!\,\Gamma(m_X + n)\Gamma(m_Y)}
$$

$$
\times \left(\frac{m_X\Omega_Y}{m_X\Omega_Y + m_Y\Omega_X}\right)^{n} g\left(m_X + n, \frac{m_X}{\Omega_X}\gamma_b\right). \quad (36)
$$

After some algebraic manipulation, the truncation error expressed in (36) can be bounded by

$$
\epsilon_{OP} \leq \left(\frac{m_Y\Omega_X}{m_X\Omega_Y + m_Y\Omega_X}\right)^{m_Y} g\left(m_X + N, \frac{m_X}{\Omega_X}\gamma_b\right)\frac{1}{\Gamma(m_Y)}
$$

$$
\times_2 F_2\left(1, m_y + N; N + 1; m_X + N; \frac{m_X\Omega_Y}{m_X\Omega_Y + m_Y\Omega_X}\right)
$$

$$
\times \frac{\Gamma(m_Y + N)}{\Gamma(m_X + N)} \left(\frac{m_X\Omega_Y}{m_X\Omega_Y + m_Y\Omega_X}\right)^{N}. \quad (37)
$$

The expression in (37) approaches zero as n approaches infinity.

VI. NUMERICAL RESULTS

In this section, we present detailed results of the BER for noncoherent and coherent detections and the OP for the shadowed BX model. The displayed figures are obtained by using the closed-form expressions given in (24) for the noncoherent BER detection, in (28) for the coherent BER detection, and in (35) for the OP. These closed-form expressions, in comparison with numerical integration, have the advantage of providing deeper insight into the effects of parameters in wireless communication systems. This enables better evaluations of system performance. In a typical wireless communication environment, it is reasonable to assume that the NLOS components have worse fading than the LOS components. We, therefore, allow the fading parameters to take values in the range $m_X \leq m_Y \leq 0.5$.

Figure 4 shows a comparison of the BER curves for the noncoherent FSK and coherent binary FSK detections as a function of the average SNR for different values of m_X. The coherent binary FSK detection is seen to have improved performance over the noncoherent detection, with both having improved system performance as the value of m_X increases. For example, the coherent detection shows approximately a 4 dB improvement for $m_X = 4$ over $m_X = 2$ at a
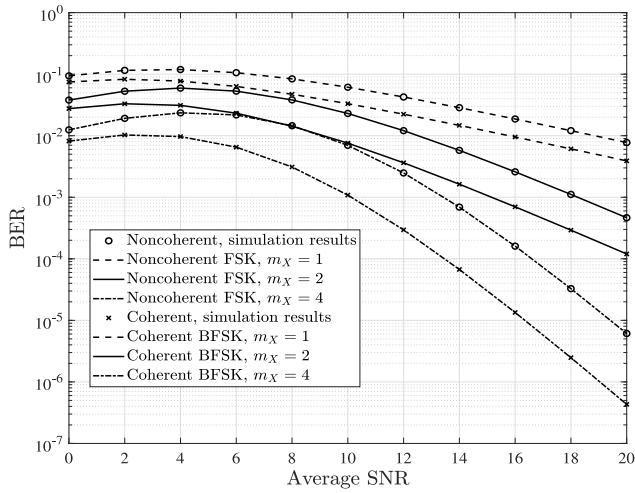
FIGURE 4. Comparison of average BER curves versus average SNR for noncoherent FSK and coherent BFSK detections over shadowed BX channels with parameters of $m_Y = 2$ and $\Omega_Y = 1$ dB.
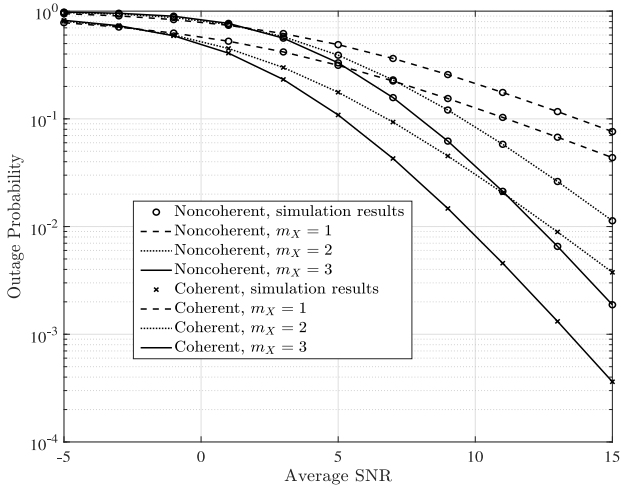
FIGURE 5. Comparison of OP curves versus average SNR for noncoherent and coherent FSK detections over shadowed BX channels with parameters of $m_Y = 2$ and $\Omega_Y = -1$ dB.

BER value of 10^{-3} with $m_Y = 2$. For noncoherent detection, a 4 dB improvement is seen for $m_X = 4$ over $m_X = 2$.

Figure 5 shows a comparison of the OP curves as a function of the average SNR for different values of m_X with consideration to noncoherent and coherent FSK detections. Improved performance is observed for coherent detection over noncoherent detection while keeping m_X constant. For example, a value of $m_X = 3$ and an OP of 10^{-2} yields a 3.5 dB improvement for coherent FSK detection over noncoherent FSK detection.

VII. CONCLUSION

In this paper, we proposed a new composite model, which we referred to as the shadowed BX model. It was based upon a recently proposed BX fading model for generalized LOS (direct and specular) components and NLOS (diffuse) components. The amplitude of the LOS component was assumed to be Nakagami-*m* distributed, which makes

its instantaneous power a Gamma RV. Such choices were made to ensure that the shadowed BX model is meaningful, according to the physical constraints of power conservation. The chief probability functions of the amplitude and power of this model were obtained in simple closed-form expressions. Closed-form expressions of average BER and OP were also obtained. Ultimately, we fit the new model to measurement data to show its flexibility and compatibility in describing various scenarios. While the experimental verification of the shadowed BX model was inconclusive, suggesting that further experimental studies are required, we were able to see the potential of both the BX and shadowed BX models. Ultimately, these models could lay the groundwork for characterizing emerging mmWave and THz wireless communication systems.

APPENDIX A
DERIVATION OF THE DIVERSITY ORDER OF THE SHADOWED BX MODEL

In this section, we derive the diversity order of the shadowed BX model by considering the derived expression for the BER for noncoherent detection as

$$\bar{P}_E = \frac{1}{2}\left(\frac{m_Y\Omega_X}{m_X\Omega_Y + m_Y\Omega_X}\right)^{m_Y}\left(\frac{m_X}{m_X + \varpi\,\Omega_X}\right)^{m_X}$$

$$\times\,_2F_1\left(m_Y, m_X; m_X; \frac{m_X^2\Omega_Y}{(m_X + \varpi\,\Omega_X)(m_X\Omega_Y + m_Y\Omega_X)}\right)$$
(38)

where $_2F_1(\cdot, \cdot; \cdot; \cdot)$ is defined as [18]

$$_2F_1(a, b; c; z) = 1 + \frac{ab}{c}z + \frac{a(1+a)b(1+b)}{c(1+c)}z^2 + \cdots;$$
$$(z \to 0). \quad (39)$$

At high SNR, the BER or OP scale according to SNR^{-N}, where N is the diversity order, meaning that a log-log plot of the BER or OP versus SNR will portray the diversity order as a slope of

$$N = -\frac{\log(\text{BER or OP})}{\log(\text{SNR})}$$
(40)

Since the Ω_X and Ω_Y are the power of the LOS and NLOS components, respectively, we can assume $\Omega_X = \Omega_Y$ and let $B = \left(\frac{m_X}{m_X + \varpi\,\Omega_X}\right)$. Applying (39) to (38) gives

$$\bar{P}_E = \frac{1}{2}\left(\frac{m_Y}{m_X + m_Y}\right)^{m_Y} B^{m_X}$$

$$\times\left[1 + \frac{m_X m_Y}{m_X + m_Y}B + \frac{m_Y(1 + m_Y)}{2}\right.$$

$$\left.\times\left(\frac{Bm_X}{m_X + m_Y}\right)^2 + \cdots\right].$$
(41)

We see that as the SNR approaches infinity, and $\Omega_X \to \infty$, we get $B \to 0$. Since $B \to 0$, $\bar{P}_E$ is dominated by first term of the square brackets in (41). Therefore,

$$\lim_{B \to 0}\bar{P}_E = \frac{1}{2}\left(\frac{m_Y}{m_X + m_Y}\right)^{m_Y} B^{m_X}$$

$$= \frac{1}{2}\left(\frac{m_Y}{m_X + m_Y}\right)^{m_Y}\left(\frac{m_X}{m_X + \varpi \Omega_X}\right)^{m_X}. \quad (42)$$

Since $\Omega_X \to \infty$, we have $m_X + \varpi \Omega_X \approx \varpi \Omega_X$. Therefore, the BER becomes

$$\lim_{\Omega_X \to \infty} \bar{P}_E = \frac{1}{2}\left(\frac{m_Y}{m_X + m_Y}\right)^{m_Y}\left(\frac{m_X}{\varpi \Omega_X}\right)^{m_X}. \quad (43)$$

This equally means

$$\bar{P}_E \propto \left(\frac{1}{\Omega_X}\right)^{m_X}. \quad (44)$$

Applying (40) to (44) leads to a diversity order of m_X for the shadowed BX model. This is expected because the diversity order is set by the small scale fading parameter.

APPENDIX B
DERIVATION OF THE BOUND ON THE TRUNCATION ERROR OF THE BER FOR COHERENT DETECTION

In this section, we derive the bound to the truncation error in (29) as given by

$$\epsilon_C = \frac{\sqrt{\varpi}}{2\sqrt{\pi}}\left(\frac{m_Y \Omega_X}{m_X \Omega_Y + m_Y \Omega_X}\right)^{m_Y}\left(\frac{m_X}{\Omega_X}\right)^{m_X}$$
$$\times \sum_{n=N}^{\infty} \frac{\Gamma(m_Y + n)}{n!\Gamma(m_Y)}\left(\frac{m_X^2 \Omega_Y}{m_X \Omega_Y + m_Y \Omega_X}\right)^n$$
$$\times \frac{\Gamma\left(m_X + n + \frac{1}{2}\right)}{\Gamma(m_X + n + 1)} \times \left(\frac{\Omega_X}{\varpi \Omega_X + m_X}\right)^{m_X + n + \frac{1}{2}}$$
$$\times_2 F_1\left(1, m_X + n + \frac{1}{2}; m_X + n + 1; \frac{m_X}{\varpi \Omega_X + m_X}\right). \quad (45)$$

It is seen that $_2F_1(1, m_X + N + \frac{1}{2}; m_X + N + 1; \frac{m_X}{\varpi \Omega_X + m_X})$ $\times(\varpi + \frac{m_X}{\Omega_X})^{-(m_X + N + \frac{1}{2})}$ decreases over n, therefore the error in the truncating series can be bounded by

$$\epsilon_C \leq \frac{\sqrt{\varpi}}{2\sqrt{\pi}\Gamma(m_Y)}\left(\frac{m_Y \Omega_X}{m_X \Omega_Y + m_Y \Omega_X}\right)^{m_Y}$$
$$\times \left(\frac{m_X}{\Omega_X}\right)^{m_X}\left(\varpi + \frac{m_X}{\Omega_X}\right)^{-\left(m_X + N + \frac{1}{2}\right)}$$
$$\times_2 F_1\left(1, m_X + N + \frac{1}{2}; m_X + N + 1; \frac{m_X}{\varpi \Omega_X + m_X}\right)$$
$$\times \sum_{n=N}^{\infty} \frac{\Gamma(m_Y + n)\Gamma\left(m_X + n + \frac{1}{2}\right)}{n!(m_X + n)\Gamma(m_X + n)}$$
$$\times \left(\frac{m_X^2 \Omega_Y}{m_X \Omega_Y + m_Y \Omega_X}\right)^n. \quad (46)$$

By a change of variable, eq. (46) becomes

$$\epsilon_C \leq \frac{\sqrt{\varpi}}{2\sqrt{\pi}\Gamma(m_Y)}\left(\frac{m_Y \Omega_X}{m_X \Omega_Y + m_Y \Omega_X}\right)^{m_Y}$$
$$\times \left(\frac{m_X}{\Omega_X}\right)^{m_X}\left(\varpi + \frac{m_X}{\Omega_X}\right)^{-\left(m_X + N + \frac{1}{2}\right)}$$

$$\times_2 F_1\left(1, m_X + N + \frac{1}{2}; m_X + N + 1; \frac{m_X}{\varpi \Omega_X + m_X}\right)$$
$$\times \sum_{j=0}^{\infty} \frac{\Gamma(m_Y + N + j)\Gamma\left(m_X + N + j + \frac{1}{2}\right)}{(N+j)!(m_X + N + j)\Gamma(m_X + N + j)}$$
$$\times \left(\frac{m_X^2 \Omega_Y}{m_X \Omega_Y + m_Y \Omega_Y}\right)^{N+j}. \quad (47)$$

Applying the definition $(a)_k = a(a+1)\cdots(a+k-1)$ to (47) gives

$$\epsilon_C \leq \frac{\sqrt{\varpi}}{2\sqrt{\pi}\Gamma(m_Y)}\left(\frac{m_Y \Omega_X}{m_X \Omega_Y + m_Y \Omega_X}\right)^{m_Y}\left(\frac{m_X}{\Omega_X}\right)^{m_X}$$
$$\times \left(\varpi + \frac{m_X}{\Omega_X}\right)^{-\left(m_X + N + \frac{1}{2}\right)}\left(\frac{m_X^2 \Omega_Y}{m_X \Omega_Y + m_Y \Omega_Y}\right)^N$$
$$\times_2 F_1\left(1, m_X + N + \frac{1}{2}; m_X + N + 1; \frac{m_X}{\varpi \Omega_X + m_X}\right)$$
$$\times \frac{\Gamma(m_Y + N - 1)\Gamma\left(m_X + N + \frac{1}{2}\right)}{\Gamma(m_X + N)}$$
$$\times \sum_{j=0}^{\infty} \frac{(m_Y + N)_j\left(m_X + N + \frac{1}{2}\right)_j}{N!(N+1)_j(m_X + N + 1)_j}$$
$$\times \left(\frac{m_X^2 \Omega_Y}{m_X \Omega_Y + m_Y \Omega_Y}\right)^j \quad (48)$$

which is equivalent to

$$\epsilon_C \leq \frac{\sqrt{\varpi}}{2\sqrt{\pi}\Gamma(m_Y)}\left(\frac{m_Y \Omega_X}{m_X \Omega_Y + m_Y \Omega_X}\right)^{m_Y}\left(\frac{m_X}{\Omega_X}\right)^{m_X}$$
$$\times \left(\varpi + \frac{m_X}{\Omega_X}\right)^{-\left(m_X + N + \frac{1}{2}\right)}\left(\frac{m_X^2 \Omega_Y}{m_X \Omega_Y + m_Y \Omega_Y}\right)^N$$
$$\times \frac{\Gamma(m_Y + N - 1)\Gamma\left(m_X + N + \frac{1}{2}\right)}{\Gamma(m_X + N)}$$
$$\times_2 F_1\left(1, m_X + N + \frac{1}{2}; m_X + N + 1; \frac{m_X}{\varpi \Omega_X + m_X}\right)$$
$$\times \sum_{n=0}^{\infty} \frac{(m_Y + N)_n\left(m_X + N + \frac{1}{2}\right)_n}{N!(N+1)_n(m_X + N + 1)_n}$$
$$\times \left(\frac{m_X^2 \Omega_Y}{m_X \Omega_Y + m_Y \Omega_Y}\right)^n. \quad (49)$$

This last result agrees with (30).

APPENDIX C
DERIVATION OF THE BOUND ON THE TRUNCATION ERROR OF THE OUTAGE PROBABILITY

In this section, we derive the bound on the truncation in (36) as given by

$$\epsilon_{OP} = \left(\frac{m_Y \Omega_X}{m_X \Omega_Y + m_Y \Omega_X}\right)^{m_Y}\sum_{n=N}^{\infty} \frac{\Gamma(m_Y + n)}{n!\Gamma(m_X + n)\Gamma(m_Y)}$$

$$\times \left(\frac{m_X \Omega_Y}{m_X \Omega_Y + m_Y \Omega_X}\right)^n g\left(m_X + n, \frac{m_X}{\Omega_X}\gamma_b\right). \quad (50)$$

It is seen that $g(m_X + n, \frac{m_X}{\Omega_X}\gamma_b)$ approaches 1 as n approaches infinity. Therefore, the error in the truncation series can be bounded by

$$\epsilon_{OP} \leq \left(\frac{m_Y \Omega_X}{m_X \Omega_Y + m_Y \Omega_X}\right)^{m_Y} g\left(m_X + N, \frac{m_X}{\Omega_X}\gamma_b\right)$$
$$\times \sum_{n=N}^{\infty} \frac{\Gamma(m_Y + n)}{n! \Gamma(m_X + n)\Gamma(m_Y)} \times \left(\frac{m_X \Omega_Y}{m_X \Omega_Y + m_Y \Omega_X}\right)^n. \quad (51)$$

By change of variable, (51) becomes

$$\epsilon_{OP} \leq \left(\frac{m_Y \Omega_X}{m_X \Omega_Y + m_Y \Omega_X}\right)^{m_Y} g\left(m_X + N, \frac{m_X}{\Omega_X}\gamma_b\right)\frac{1}{\Gamma(m_Y)}$$
$$\times \sum_{j=0}^{\infty} \frac{\Gamma(m_Y + N + j)}{(N+j)! \Gamma(m_X + N + j)}\left(\frac{m_X \Omega_Y}{m_X \Omega_Y + m_Y \Omega_X}\right)^{N+j}. \quad (52)$$

Applying the definition $(a)_k = a(a+1)\cdots(a+k-1)$ to (52) gives

$$\epsilon_{OP} \leq \left(\frac{m_Y \Omega_X}{m_X \Omega_Y + m_Y \Omega_X}\right)^{m_Y} g\left(m_X + N, \frac{m_X}{\Omega_X}\gamma_b\right)\frac{1}{\Gamma(m_Y)}$$
$$\times \frac{\Gamma(m_Y + N)}{\Gamma(m_X + N)}\left(\frac{m_X \Omega_Y}{m_X \Omega_Y + m_Y \Omega_X}\right)^N$$
$$\times \sum_{j=0}^{\infty} \frac{(m_Y + N)_j (1)_j}{N! (m_X + N)_j (N+1)_j}\left(\frac{m_X \Omega_Y}{m_X \Omega_Y + m_Y \Omega_X}\right)^j \quad (53)$$

which is equivalent to

$$\epsilon_{OP} \leq \left(\frac{m_Y \Omega_X}{m_X \Omega_Y + m_Y \Omega_X}\right)^{m_Y} g\left(m_X + N, \frac{m_X}{\Omega_X}\gamma_b\right)\frac{1}{\Gamma(m_Y)}$$
$$\times \frac{\Gamma(m_Y + N)}{\Gamma(m_X + N)}\left(\frac{m_X \Omega_Y}{m_X \Omega_Y + m_Y \Omega_X}\right)^N$$
$$\times \sum_{n=0}^{\infty} \frac{(m_Y + N)_n (1)_n}{N! (m_X + N)_n (N+1)_n}\left(\frac{m_X \Omega_Y}{m_X \Omega_Y + m_Y \Omega_X}\right)^n. \quad (54)$$

The result in (54) agrees with (37).

REFERENCES

[1] J. Naylon. (2016). *2016 Predictions: Why 5G, Demand for Spectrum and Increased Capacity Will Drive Operator Strategies*. Accessed: Dec. 4, 2018. [Online]. Available: https://www.rcrwireless.com/2016 0111/opinion/2016-predictions-why-5g-demand-for-spectrum-and-incr eased-capacity-will-drive-operator-strategies-tag10

[2] G. D. Durgin, T. S. Rappaport, and D. A. de Wolf, "New analytical models and probability density functions for fading in wireless communications," *IEEE Trans. Commun.*, vol. 50, no. 6, pp. 1005–1015, Jun. 2002.

[3] M. K. Samimi, G. R. MacCartney, S. Sun, and T. S. Rappaport, "28 GHz millimeter-wave ultrawideband small-scale fading models in wireless channels," in *Proc. IEEE 83rd Veh. Technol. Conf. (VTC Spring)*, Nanjing, China, May 2016, pp. 1–6.

[4] X. Wang and N. C. Beaulieu, "Switching rates of two-branch selection diversity in κ-μ and α-μ distributed fadings," *IEEE Trans. Wireless Commun.*, vol. 8, no. 4, pp. 1667–1671, Apr. 2009.

[5] A. Olutayo, H. Ma, J. Cheng, and J. F. Holzman, "Level crossing rate and average fade duration for the Beaulieu-Xie fading model," *IEEE Wireless Commun. Lett.*, vol. 6, no. 3, pp. 326–329, Jun. 2017.

[6] N. C. Beaulieu and J. Xie, "A novel fading model for channels with multiple dominant specular components," *IEEE Wireless Commun. Lett.*, vol. 4, no. 1, pp. 54–57, Feb. 2015.

[7] A. Goldsmith, *Wireless Communication*. New York, NY, USA: Cambridge Univ. Press, 2004.

[8] M. D. Yacoub, "Nakagami-*m* phase–envelope joint distribution: A new model," *IEEE Trans. Veh. Technol.*, vol. 59, no. 3, pp. 1552–1557, Mar. 2010.

[9] N. C. Beaulieu and S. A. Saberali, "A generalized diffuse scatter plus line-of-sight fading channel model," in *Proc. IEEE Int. Conf. Commun. (ICC)*, Sydney, NSW, Australia, Jun. 2014, pp. 5849–5853.

[10] S. Wyne, A. P. Singh, F. Tufvesson, and A. F. Molisch, "A statistical model for indoor office wireless sensor channels," *IEEE Trans. Wireless Commun.*, vol. 8, no. 8, pp. 4154–4164, Aug. 2009.

[11] M. Rao, F. J. Lopez-Martinez, M. S. Alouini, and A. Goldsmith, "MGF approach to the analysis of generalized two-ray fading model," *IEEE Trans. Wireless Commun.*, vol. 14, no. 5, pp. 2548–2561, May 2015.

[12] A. Abdi, W. C. Lau, M. S. Alouini, and M. Kaveh, "A new simple model for land mobile satellite channels: First- and second-order statistics," *IEEE Trans. Wireless Commun.*, vol. 2, no. 3, pp. 519–528, May 2003.

[13] J. M. Romero-Jerez, F. J. Lopez-Martinez, J. F. Paris, and A. J. Goldsmith, "The fluctuating two-ray fading model: Statistical characterization and performance analysis," *IEEE Trans. Wireless Commun.*, vol. 16, no. 7, pp. 4420–4432, Jul. 2017.

[14] J. F. Paris, "Statistical characterization of κ-μ shadowed fading," *IEEE Trans. Veh. Technol.*, vol. 63, no. 2, pp. 518–520, Feb. 2014.

[15] C. Loo, "A statistical model for a land mobile satellite link," *IEEE Trans. Veh. Technol.*, vol. 34, no. 3, pp. 122–127, Aug. 1985.

[16] I. S. Gradshteyn and I. M. Ryzhik, *Table of Integrals, Series, and Products*, 6th ed. New York, NY, USA: Academic, 2000.

[17] F. J. Lopez-Martinez, J. F. Paris, and J. M. Romero-Jerez, "The κ-μ shadowed fading model with integer fading parameters," *IEEE Trans. Veh. Technol.*, vol. 66, no. 9, pp. 7653–7662, Sep. 2017.

[18] E. W. Weisstein. (1999). *Hypergeometric Function*. [Online]. Available: https://mathworld.wolfram.com/HypergeometricFunction. html

[19] V. A. Aalo and J. Zhang, "Performance analysis of maximal ratio combining in the presence of multiple equal-power cochannel interferers in a Nakagami fading channel," *IEEE Trans. Veh. Technol.*, vol. 50, no. 2, pp. 497–503, Mar. 2001.

[20] M. Abramowitz and I. A. Stegun, *Handbook of Mathematical Functions With Formulas, Graphs and Mathematical Tables*, 10th ed. New York, NY, USA: Dover Publ., 1972.

[21] W. Magnus, F. Oberhettinger, and R. P. Soni, *Formulas and Theorems for the Special Functions of Mathematical Physics*, 3rd ed. New York, NY, USA: Springer, 1966.

[22] A. Papoulis, *Probability, Random Variables and Stochastic Processes*. New York, NY, USA: McGraw-Hill, 1994.

[23] E. W. Weisstein. (1999). *Confluent Hypergeometric Function of the First Kind*. [Online]. Available: http://mathworld.wolfram.com/ ConfluentHypergeometricFunctionoftheFirstKind.html

[24] A. Naimi and G. Azemi, "Moment-based Ricean *K*-factor estimation in the presence of shadowing," in *Proc. 9th Int. Symp. Signal Process. Appl.*, Sharjah, UAE, Feb. 2007, pp. 1–4.

[25] A. K. Majumdar, *Optical Wireless Communications for Broadband Global Internet Connectivity: Fundamentals and Potential Applications*. Amsterdam, The Netherlands: Elsevier, 2019.

[26] C. Tepedelenlioglu, A. Abdi, and G. B. Giannakis, "The Ricean *K*-factor: Estimation and performance analysis," *IEEE Trans. Wireless Commun.*, vol. 2, no. 4, pp. 799–810, Jul. 2003.

[27] J. S. Butterworth and E. E. Matt, "The characterization of propagation effects for land mobile satellite services," in *Proc. IEEE Satellite Syst. Mobile Commun. Navig.*, London, U.K., Jun. 1983, pp. 51–54.